

# Band-gap engineering by contact geometry in graphene nanoribbons: Experimental and theoretical studies on artificial materials

Thomas Stegmann,<sup>1,\*</sup> John A. Franco-Villafañe,<sup>2,1</sup> Ulrich Kuhl,<sup>3</sup> Fabrice Mortessagne,<sup>3</sup> and Thomas H. Seligman<sup>1,4</sup>

<sup>1</sup>*Instituto de Ciencias Físicas, Universidad Nacional Autónoma de México, 62210 Cuernavaca, México*

<sup>2</sup>*CONACYT - Instituto de Física, Universidad Autónoma de San Luis Potosí, San Luis Potosí, SLP 78290, México*

<sup>3</sup>*Université Nice Sophia Antipolis, CNRS, Laboratoire de Physique de la Matière Condensée, UMR 7336, 06100 Nice, France*

<sup>4</sup>*Centro Internacional de Ciencias, 62210 Cuernavaca, México*

(Dated: September 28, 2016)

Electron transport in small graphene nanoribbons is studied by microwave emulation experiments and tight-binding calculations. In particular, it is investigated under which conditions a transport band-gap can be observed. Our experiments provide evidence that armchair ribbons of width  $3m+2$  with integer  $m$  are metallic and otherwise semiconducting, whereas zigzag ribbons are metallic independent of their width. The contact geometry, defining to which atoms at the ribbon edges the source and drain leads are attached, has strong effects on the transport. If leads are attached only to the inner atoms of zigzag edges, broad transport band-gaps can be observed in all armchair ribbons as well as in rhomboid-shaped zigzag ribbons. All experimental results agree qualitatively with tight-binding calculations using the nonequilibrium Green's function method.

PACS numbers: 73.63.-b, 72.80.Vp, 73.23.-b

## I. INTRODUCTION & OUTLINE

Nowadays, graphene is one of the most studied materials in condensed matter physics because of its various exceptional properties and their technical applications, see Refs. 1–8 for an overview. One of the most remarkable features is that graphene has a linear dispersion relation at the Dirac points, which lets the electrons behave as relativistic, massless, charged fermions. The high mobility of the charge carriers, coming from the special dispersion relation at the Fermi energy, makes graphene very promising for new electronic devices. However, the absence of a band-gap in graphene inhibits to substitute nowadays silicon-based semiconductor technology by graphene.<sup>9</sup> One approach to open a band-gap in graphene is to use nanoribbons, i.e. small stripes of graphene, see Figure 1. On one hand, this approach has the advantage that the rather small size of graphene nanoribbons may lead to a high miniaturization and integration of these devices. On the other hand, it has the disadvantage that it is still challenging to produce nanoribbons of well controlled size and geometry, although there is promising progress, see for example Refs. 10–17. Moreover, connecting nanoribbons to leads, where electrons are injected and extracted, is experimentally demanding.

Recently, it has been shown that a tight-binding model of graphene and polyacetylene can be emulated by microwave experiments.<sup>18–21</sup> Such experiments are well controlled and easily to perform (in comparison to experiments with real graphene or polyacetylene) and hence, offer a versatile tool to investigate in detail the properties of these systems. In this article, we study the ballistic single-electron transport through small graphene nanoribbons by microwave transmission experiments. Our measurements are supported by tight-binding calculations using the nonequilibrium Green's function (NEGF) method.<sup>22–24</sup>

Graphene nanoribbons have two elementary edge structures, the zigzag and the armchair shape, see for example the horizontal edges in Figure 1 (a) and (b), respectively. Edge deformations are not considered here.<sup>25</sup> Studies of graphene nanoribbons<sup>26–30</sup> predict that armchair ribbons of width  $3m+2$  with integer  $m$  are metallic and otherwise semiconducting, i.e. they show a broad transport band-gap at the Dirac point.<sup>31</sup> Zigzag ribbons are predicted to be metallic for all ribbon widths. First samples of small graphene nanoribbons have been synthesized recently<sup>10–17</sup> indicating the predicted behavior. Here, we present emulation experiments of the electronic transport through small nanoribbons with specific edges and atomically precise connections to source and drain leads. We do not only provide further evidence to the predicted behavior but study also the effect of the contact geometry, which determines to which sites at the edges of the ribbons leads are attached. We show that by tuning the contact geometries, broad transmission band-gaps can be induced in graphene nanoribbons with armchair and zigzag edges independent from their actual width. Contact effects on the transport in graphene nanoribbons have been addressed only rarely. Square lattices have been attached to the honeycomb lattice of graphene ribbons,<sup>32–36</sup> which for example induces in zigzag ribbons of even width a band-gap, while ribbons of odd width remain metallic. Similar even-odd parity effects can be observed also with respect to the total length of the ribbon.<sup>37</sup> The case where leads are attached to small<sup>38,39</sup> and larger<sup>40</sup> nanoribbons has also been studied.

The paper is organized as follows. In Section II, we describe the studied systems and explain briefly the used experimental and theoretical methods. Our results are presented and discussed in Section III. Conclusions and an outlook can be found in Section IV.

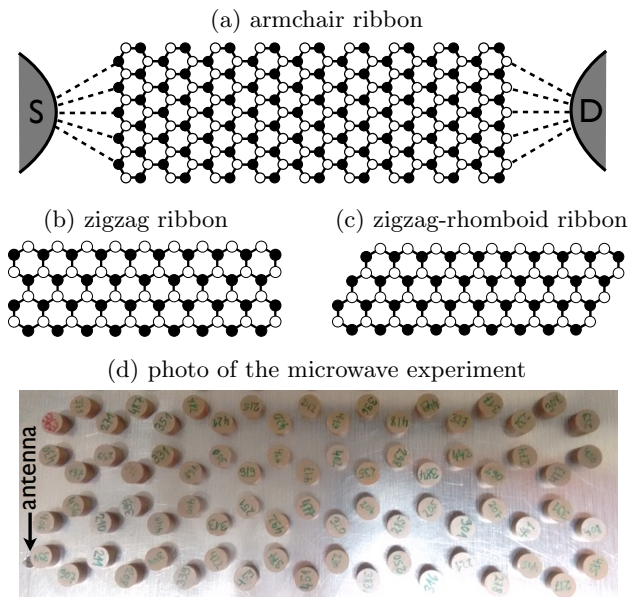


Figure 1. Electron transport through graphene nanoribbons from source (S) to drain (D) is studied by microwave emulation experiments and tight-binding calculations. Panel (a) shows an armchair ribbon of width 5, while zigzag and zigzag-rhomboid ribbons of width 3 are displayed in panel (b) and (c), respectively. The black and white color shading of the resonators indicate the two different sublattices to which the atoms belong. The contact geometry, i.e the way how source and drain are coupled to the ribbon (dashed lines), has important effects on the transport. Panel (d) shows a photo of the experimental setup for a zigzag ribbon of width 3. On the left hand side the antenna on the bottom plate is seen, whereas the antenna on the right hand side is mounted to the top plate (not shown).

## II. SYSTEM & METHODS

We consider graphene nanoribbons of the types shown in Figure 1, namely an armchair ribbon (a), a zigzag ribbon (b) and a zigzag-rhomboid ribbon (c). The naming of the ribbons is due to the shape of their horizontal edges and, in the case of Figure 1 (c), due to the overall shape of the ribbon. Because of experimental limitations, the length of the ribbons is kept as shown in Figure 1, while their width is varied. However, calculations have been performed also for larger systems, giving qualitatively the same results discussed below. Leads through which electron (or microwaves) are injected and extracted, are attached to the atoms at the left and right edges, see the dashed lines in Figure 1 (a).

### A. Microwave experiment

Applying the techniques, developed to investigate the band structure of graphene<sup>18,19</sup> and to emulate relativistic systems<sup>41,42</sup> as well as molecular systems<sup>21</sup>, we have performed analogous experiments to study the coherent

transport in graphene nanoribbons.

A set of identical dielectric cylindrical resonators (5 mm height, 4 mm radius, refractive index  $n \approx 6$ ) is placed between two metallic plates. A photo of the experimental setup without the top plate is shown in Figure 1 (d). The individual resonators have an isolated resonance at  $\nu'_0 = 6.655 \pm 0.005$  GHz, corresponding to the lowest transverse electric (TE) mode. We restrict our investigation to frequencies around  $\nu'_0$ , where each resonator contributes only one resonance. The nearest neighbor distance between the center of the resonators is  $d_1 = 12.0$  mm. The dielectric resonators play the role of the carbon atoms in the ribbons, while the electromagnetic waves corresponds to the wave function of the electron. A detailed description of the experimental setup can be found in Ref. 19. As the antennas are positioned always close to or above a single resonator they couple to the closest resonator only, thus measuring the transmission from an individual resonator on the left hand side to another individual resonator at the right hand side. By changing the antenna positions all combinations of transmission between edge resonators are measured. Due to the weak coupling of the antennas the total transmission is then given by summing up all contributions, see Section II B. As the system is time-reversal invariant the transmission is reciprocal, i.e. the transport in both directions is the same.

### B. Tight-binding transport calculations

Theoretically, the graphene nanoribbons are described by the tight-binding Hamiltonian

$$H = \sum_{|i-j| \leq 3nn} t_{|i-j|} |i\rangle \langle j|. \quad (1)$$

The coupling parameters  $t_{|i-j|}$ , which have been obtained by fitting our calculations to the experimental data, are given in Table I. In the sum in Equation (1), interactions up to third nearest neighbors (3nn) are taken into account. Interactions to higher nearest neighbors can be safely ignored due to the large distance of these sites and the additional screening by the closer sites.

	$t_1$	$t_2$	$t_3$
	39.5	5.0	3.0

Table I. Coupling parameters  $t_i$  (in MHz) up to third nearest neighbors. The three parameters have been obtained by fitting our calculations to the experimental data.

From now on we will use the normalized frequency  $\nu = \nu' - \nu'_0 - 3t_2$ , where the Dirac point is located theoretically<sup>43</sup> in the center of the transmission band (i.e. at  $\nu = 0$ ).

The electron transport through the nanoribbons is calculated by means of the nonequilibrium Green's function (NEGF) method. In the following, we briefly summarize the essential equations. Details can be found in Refs. 22–24. The Green's function of the chain is defined as

$$G(\nu) = \left[ \nu - H - \Sigma_S - \Sigma_D - \Sigma_{\text{abs}} - \Sigma_{\text{dis}} \right]^{-1}, \quad (2)$$

where  $\nu$  is the electron energy corresponding to the microwave frequency in the experiment.

The effect of the source and drain leads by which electrons are injected and extracted, is described by the self-energies

$$\Sigma_S = -i\eta \sum_{i \in S} |i\rangle \langle i|, \quad \Sigma_D = -i\eta \sum_{i \in D} |i\rangle \langle i|. \quad (3)$$

The coupling strength  $\eta = 0.6 \text{ MHz}$  is adjusted to the experiment. The sums are over the sites where leads are attached, see for example in Figure 1 (a) the sites which are connected by dashed lines to the source and drain, respectively. The sites connected to leads are also indicated in the insets of figures 2, 4 and 5 by the black sites. The self-energies show no coherences, i.e. no off-diagonal elements, which is justified because in the experiment the antennas are coupled only weakly to the resonators.

Absorption, which is present in the experiment, is modeled by the imaginary potential (or self-energy)

$$\Sigma_{\text{abs}} = -i\gamma(W) \sum_{i=1}^N |i\rangle \langle i|, \quad (4)$$

where  $N$  is the total number of sites of the ribbon. We obtain best agreement between the experimental data and the calculations using for the armchair ribbons a linear decay of the absorption  $\frac{\gamma(W)}{\text{MHz}} = 0.99 - 0.06W$ , where  $W$  is the width of the ribbon measured in multiples of the hexagonal cell size. For the zigzag and zigzag-rhomboid ribbons, we use a constant absorption  $\gamma(W) = 0.99 \text{ MHz}$ .

In the experiment, some degree of disorder cannot be avoided completely due to the uncertainty of the resonance frequency of the resonators and the uncertainty of their positions. In the calculations, disorder is taken into account by a random potential (or self-energy)

$$\Sigma_{\text{dis}} = \sum_{i=1}^N \epsilon_i |i\rangle \langle i|, \quad (5)$$

where the  $\epsilon_i$  are chosen from a Gaussian distribution which is cut at its full width half maximum, which corresponds approximately to the experimentally observed distribution and the used selection rule. We consider the standard deviation  $\sigma = 10 \text{ MHz}$  and an ensemble of  $10^2$  realizations.

The transmission between source and drain is then given by

$$\begin{aligned} T(\nu) &= 4\text{Tr} \left( \text{Im}(\Sigma_S) G \text{Im}(\Sigma_D) G^\dagger \right) \\ &= \sum_{i \in S, j \in D} T_{ij}. \end{aligned} \quad (6)$$

where  $T_{ij}(\nu) = 4\eta^2 |G_{ij}|^2$  is the transmission between an individual site  $i$  at the left end of the ribbon to another site  $j$  at the right end. As discussed in Section II A, these functions  $T_{ij}$  are measured in the microwave experiment. Note that in the last step in Equation (6), we have used the fact that the self-energies in Equation (3) describing the effect of source and drain are sparse matrices with only some non-vanishing entries on their diagonals.

In order to understand the transport properties, we will also calculate the local density of states (LDOS)

$$D(\nu) = \text{Diag} \left( G [\Sigma_S + \Sigma_D] G^\dagger \right). \quad (7)$$

Due to the weak coupling of the leads to the nanoribbon, see Equation (3), the LDOS is very similar to the eigenstates of the closed Hamiltonian in Equation (1), which are near to the considered frequency. Contact induced states<sup>44</sup> have only minor effects here.

### III. RESULTS & DISCUSSION

#### A. Armchair ribbons

The transmission through graphene armchair ribbons for various widths and contact geometries is shown in Figure 2. Experimental data are indicated by the blue-solid curves while our tight-binding calculations are highlighted by the red-dashed curves. The narrow ribbons are sketched in the insets, where the black shaded sites are connected to leads.

We observe that in all ribbons the conductivity decreases when the Dirac point around  $\nu = 0$  is approached. In the first row the leads are attached to all atoms at the confining zigzag edges to the left and right. For ribbons of width  $3m+2$  with integer  $m$  (i.e. widths 2 and 5 in Figure 2), the conductivity around the Dirac point is low but finite. These ribbons are metallic in the whole transmission band ranging approximately from  $-80$  to  $160 \text{ MHz}$ . For ribbons of other widths (i.e. widths 1, 3 and 4 in Figure 2) the conductivity around the band-center approaches zero. A transport band-gap (gray shaded regions) opens in these ribbons, which hence are semiconducting. We therefore provide clear experimental evidence of this theoretically predicted<sup>2,26–30,45</sup> behavior of graphene armchair ribbons. In general, the tight-binding calculations agree well with the experimental data. In the upper part of the conduction band (from 0 to  $160 \text{ MHz}$ ) almost all resonance peaks coincide. In the lower part (from  $-80$  to  $0 \text{ MHz}$ ) the agreement is not that perfect but the general trend of the experimental data is reproduced also there. Differences between experiment and theory are more notorious in the band-gap than outside. In particular for certain ribbon width the experiment shows peaks which are not present in our calculations and which we attribute to localized states enhanced by irregularities of the experimental setup.

The differences between the metallic and semiconducting armchair ribbons become more pronounced if the

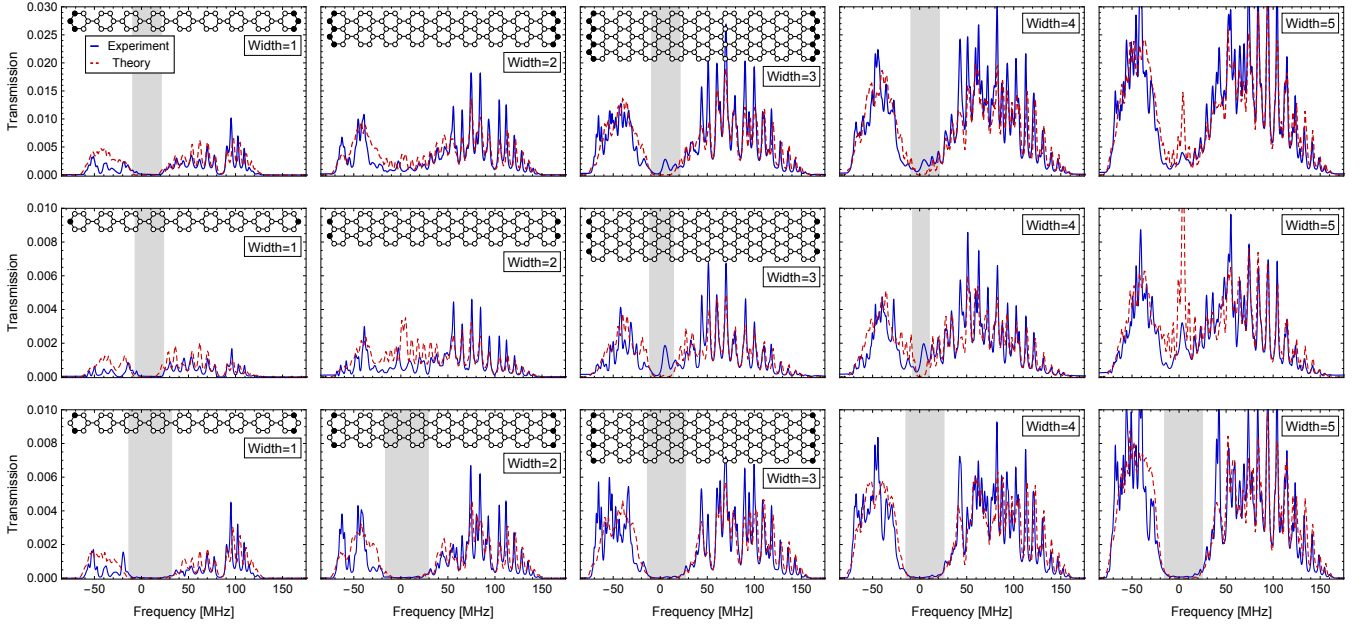


Figure 2. Transmission through armchair graphene nanoribbons of length 9 and for increasing widths (from left to right). The ribbons up to a width of 3 are sketched in the insets. The leads (or antenna) through which electrons (or microwaves) are injected and extracted are connected to the black sites at the edges of the ribbons. Experimental data is shown by blue-solid lines, while our tight-binding Green's function calculations are indicated by red-dashed lines. First row: Connecting leads to all atoms on the zigzag edges, we confirm that the ribbons of width 2 and 5 are metallic, while otherwise the ribbons show a band-gap (gray shaded regions) around  $\nu = 0$ . Second row: Connecting only the outer atoms on the zigzag edges, see the black marked atoms in the insets, the differences between the metallic (width 2 and 5) and semiconducting (width 1, 3 and 4) ribbons become more pronounced. Third row: Connecting only the inner atoms of the zigzag edges to leads, we find a broad band-gap for all ribbon widths.

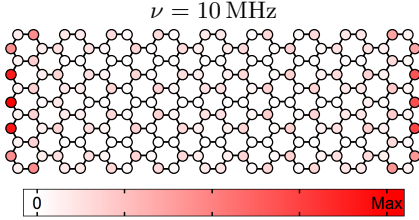


Figure 3. Calculated LDOS  $D(\nu)$  in the armchair ribbon indicated by the color-shading of the resonators. Close to the Dirac point, the LDOS vanishes on the inner atoms of the confining zigzag edges to the left and right, while it is non-zero on the outer atoms. Note that leads are attached to all sites at the confining zigzag edges to the left and right.

leads are attached only to the outer atoms of the confining zigzag edges, see the second row in Figure 2. The transport through the ribbons changes drastically, if the leads are attached only to the inner atoms, as shown in the third row of Figure 2. In this case a clearly pronounced transport band-gap is observed for all armchair ribbons, independent from their actual width.

In order to understand the effects of the contact geometry on the transport, we show in Figure 3 the local density of states (LDOS), which has been calculated by means of Equation (7), near to  $\nu = 0$  where the band-

gap appears. At the zigzag edges to the left and right, where the leads are attached, the LDOS is localized on the outer atoms, whereas it vanishes on the inner atoms. This property can be observed for all frequencies within the band-gap. Thus, the inner atoms on zigzag edges are essentially insulating and broad transport band-gaps (gray shaded regions) can be observed, if the leads are attached only to these atoms. The confining zigzag edges of the studied finite armchair nanoribbons stamp their fingerprint on the transport and can suppress the metallicity in armchair ribbons.

The behavior of the LDOS in Figure 3 can be understood by the sublattice structure of graphene.<sup>2,28,45</sup> At zigzag edges, see for example in Figure 1 (a) the edge to the left hand side, all inner atoms belong to one sublattice A (white resonators), whereas all outer atoms belong to the other sublattice B (black resonators). If the nanoribbon is extended hypothetically by one layer of atoms into the region, where the wave function has to vanish due to hard-wall boundary conditions, all these atoms would belong to sublattice A only. Thus, at a zigzag edge the wave function has to vanish on the sublattice to which also the inner atoms belong, whereas no constraint has to be fulfilled by the wave function for the sublattice of the outer atoms. This makes it possible that on the outer atoms of zigzag edges a edge (or surface) state can reside,

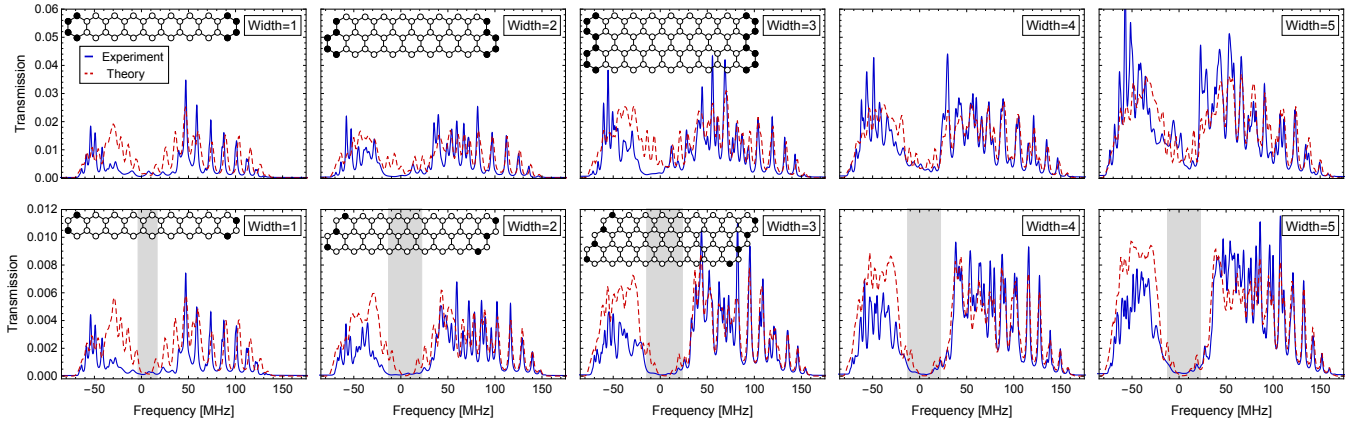


Figure 4. Transmission through zigzag and zigzag-rhomboid ribbons of length 9 and increasing width (from left to right). The more narrow ribbons are sketched in the insets. The leads are attached to the black sites. Top row: Connecting leads to all atoms at the confining armchair edges to the left and right, we observe that all zigzag ribbons are metallic. Bottom row: If leads are connected to the inner atoms of a zigzag-rhomboid ribbon, broad transmission band-gaps (gray shaded regions) can be observed for all ribbons.

while the wave function vanishes essentially on the inner atoms. Moreover, the surface states are localized on one of the two  $K$  points, which makes them robust against perturbations.<sup>2,26–30,45</sup> Note that the localization of the edge states on the outer atoms of graphene zigzag edges can be understood also from a simple resonance theoretic picture as well as from valence bond and molecular orbit theory.<sup>46</sup> These edge states have been observed in microwave experiments.<sup>47</sup> Take into account that connecting leads to the inner atoms on the zigzag edges is not equivalent to removing the outer atoms. This would lead to beard edges, which have edge states and show different transport properties.<sup>47</sup>

## B. Zigzag ribbons

The transmission through zigzag ribbons is shown in Figure 4 (top row). The leads are attached to the inner and outer atoms of the confining armchair edges, see the black shaded sites of the nanoribbons sketched in the insets. Experimental data are shown by blue-solid curves, calculations by red-dashed curves.

As in Figure 2, the transmission decreases when the Dirac point around  $\nu = 0$  is approached but it remains finite for all ribbons. In agreement with theoretical predictions,<sup>2,27–30,45</sup> all zigzag ribbons behave metallic independent from their actual width.

In zigzag ribbons a band-gap cannot be opened by contact engineering. The calculated LDOS in Figure 5 (left) close to  $\nu = 0$  is finite for all atoms on the confining armchair edges to the left and right hand side, because atoms from both sublattices appear there, see the alternating black and white resonators in Figure 1 (b). A surface (or edge) state does not exist at armchair edges. This behavior can be observed for all frequencies close to  $\nu = 0$ . Moreover, solving the corresponding Dirac equation, the wave function is located

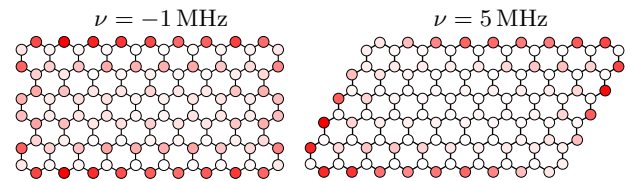


Figure 5. Left: In the zigzag ribbon the calculated LDOS is non-vanishing on all atoms of the confining armchair edges, where the leads are attached. A band-gap cannot be induced by contact engineering. Right: At the edges of the zigzag-rhomboid ribbon, the calculated LDOS is located on the outer atoms and vanishes on the inner atoms.

on both  $K$  points (valley mixing), which makes it sensitive to perturbations.<sup>2,28,45</sup> Note that for the ribbons of width 2 and 3, the experiment shows a small band-gap, which is up to now not understood and not observed in our theoretical calculations.

In the zigzag-rhomboid ribbons, depicted for example in Figure 1 (c), all edges have the zigzag shape. This allows to tune the transport in the system by suitable contact geometries. Close to the Dirac point the calculated LDOS in Figure 5 (right) is located on the outer atoms of the zigzag edges whereas it vanishes on the inner atoms. Therefore, if the leads are attached to the inner atoms of the edges to the left and right hand side, see Figure 4 (bottom row), a broad transmission band-gap is observed. These band-gaps are observed for all ribbons independent from their size.

## IV. CONCLUSIONS & OUTLOOK

In this paper, the electronic transport in graphene nanoribbons has been studied by microwave emulation experiments and tight-binding Green's function calculations. The microwave experiment emulates only the bal-



listic single-particle transport. Correlations due to interactions between the electrons, which may be present in real graphene, cannot be taken into account.

We have presented experimental evidence that the width of armchair ribbons determines whether the ribbon is metallic or semiconducting, see Figure 2 (top row). We have also shown that all (rectangular-shaped) zigzag ribbons are metallic, independent from their actual size, see Figure 4 (top row).

We have found that the transport properties can be tuned by the contact geometry, using the fact that the zigzag edge state resides on the outer atoms but not on the inner atoms, see the local density of states in Figure 3 and Figure 5. Hence, broad transmission bandgaps can be induced in those ribbons, where the leads are attached to the inner atoms of zigzag edges, see the armchair ribbons in Figure 2 (bottom row) as well as the zigzag-rhomboid ribbons in Figure 4 (bottom row). The realization of such contact geometries may be extremely difficult in real graphene. However, considering the recent progress,<sup>10–17</sup> we think that this can be possible in the near future. Our microwave emulation experiments thus may be viewed as a testing ground for new concepts.

In the future, we plan to investigate in more detail the transport in rhomboid-shaped ribbons, where the contacts are attached to the corners. For example, it has been predicted theoretically<sup>48,49</sup> that in zigzag-rhomboid ribbons at the Dirac point the 60° corners are conducting, while 120° corners are insulating. This theory can be confirmed by the local density of states in Figure 5 (right). However, first experiments show surprisingly strong discrepancies to our tight-binding calculations, which we cannot explain at this point and require further studies.

## ACKNOWLEDGMENTS

We thank N. Szpak for fruitful discussions and his comments about the manuscript. Financial support from CONACyT research grant 219993 and PAPIIT-DGAPA-UNAM research grants IG100616 and IN114014 is acknowledged. T.S. acknowledges a postdoctoral fellowship from DGAPA-UNAM. T.H.S. and J.A.F.-V. are grateful for the hospitality regularly received at the LPMC.

- 
- \* stegmann@icf.unam.mx
- <sup>1</sup> A. K. Geim, *Science* **324**, 1530 (2009).
  - <sup>2</sup> A. H. Castro Neto, F. Guinea, N. M. R. Peres, K. S. Novoselov, and A. K. Geim, *Rev. Mod. Phys.* **81**, 109 (2009).
  - <sup>3</sup> P. Avouris, *Nano Lett.* **10**, 4285 (2010).
  - <sup>4</sup> K. S. Novoselov, V. I. Fal'ko, L. Colombo, P. R. Gellert, M. G. Schwab, and K. Kim, *Nature* **490**, 192 (2012).
  - <sup>5</sup> M. Katsnelson, *Graphene: Carbon in two dimensions* (Cambridge University Press, 2012).
  - <sup>6</sup> A. C. Ferrari *et al.*, *Nanoscale* **7**, 4598 (2015).
  - <sup>7</sup> H. Aoki and M. S. Dresselhaus, eds., *Physics of Graphene* (Springer, 2014).
  - <sup>8</sup> L. E. F. Foa Torres, S. Roche, and J.-C. Charlier, *Introduction to graphene-based nanomaterials: from electronic structure to quantum transport* (Cambridge University Press, 2014).
  - <sup>9</sup> F. Schwierz, *Nat. Nano* **5**, 487 (2010).
  - <sup>10</sup> J. Cai, P. Ruffieux, R. Jaafar, M. Bieri, T. Braun, S. Blankenburg, M. Muoth, A. P. Seitsonen, M. Saleh, X. Feng, K. Müllen, and R. Fasel, *Nature* **466**, 470 (2010).
  - <sup>11</sup> M. Koch, F. Ample, C. Joachim, and L. Grill, *Nat. Nano* **7**, 713 (2012).
  - <sup>12</sup> P. Ruffieux, J. Cai, N. C. Plumb, L. Patthey, D. Prezzi, A. Ferretti, E. Molinari, X. Feng, K. Müllen, C. A. Pignedoli, and R. Fasel, *ACS Nano* **6**, 6930 (2012).
  - <sup>13</sup> Y.-C. Chen, D. G. de Oteyza, Z. Pedramrazi, C. Chen, F. R. Fischer, and M. F. Crommie, *ACS Nano* **7**, 6123 (2013).
  - <sup>14</sup> J. Cai, C. A. Pignedoli, L. Talirz, P. Ruffieux, H. Söde, L. Liang, V. Meunier, R. Berger, R. Li, X. Feng, K. Müllen, and R. Fasel, *Nat. Nano* **9**, 896 (2014).
  - <sup>15</sup> Y.-C. Chen, T. Cao, C. Chen, Z. Pedramrazi, D. Haberer, D. G. de Oteyza, F. R. Fischer, S. G. Louie, and M. F. Crommie, *Nat. Nano* **10**, 156 (2015).
  - <sup>16</sup> A. Kimouche, M. M. Ervasti, R. Drost, S. Halonen, A. Harju, P. M. Joensuu, J. Sainio, and P. Liljeroth, *Nat. Commun.* **6**, 10177 (2015).
  - <sup>17</sup> P. Ruffieux, S. Wang, B. Yang, C. Sánchez-Sánchez, J. Liu, T. Dienel, L. Talirz, P. Shinde, C. A. Pignedoli, D. Passerone, T. Dumlaff, X. Feng, K. Müllen, and R. Fasel, *Nature* **531**, 489 (2016).
  - <sup>18</sup> M. Bellec, U. Kuhl, G. Montambaux, and F. Mortessagne, *Phys. Rev. Lett.* **110**, 033902 (2013).
  - <sup>19</sup> M. Bellec, U. Kuhl, G. Montambaux, and F. Mortessagne, *Phys. Rev. B* **88**, 115437 (2013).
  - <sup>20</sup> S. Barkhofen, M. Bellec, U. Kuhl, and F. Mortessagne, *Phys. Rev. B* **87**, 035101 (2013).
  - <sup>21</sup> T. Stegmann, J. A. Franco-Villafañe, Y. P. Ortiz, U. Kuhl, F. Mortessagne, and T. H. Seligman, "Microwave emulations and tight-binding calculations of transport in polyacetylene," accepted by *Phys. Lett. A*, arxiv:1601.07491.
  - <sup>22</sup> S. Datta, *Electronic Transport in Mesoscopic Systems* (Cambridge University Press, 1997).
  - <sup>23</sup> S. Datta, *Quantum Transport: Atom to Transistor* (Cambridge University Press, 2005).
  - <sup>24</sup> C. H. Lewenkopf and E. R. Mucciolo, *J. Comput. Electron.* **12**, 203 (2013).
  - <sup>25</sup> P. Hawkins, M. Begliarbekov, M. Zivkovic, S. Strauf, and C. P. Search, *J. Phys. Chem. C* **116**, 18382 (2012).
  - <sup>26</sup> M. Fujita, K. Wakabayashi, K. Nakada, and K. Kusakabe, *J. Phys. Soc. Jpn.* **65**, 1920 (1996).
  - <sup>27</sup> K. Nakada, M. Fujita, G. Dresselhaus, and M. S. Dresselhaus, *Phys. Rev. B* **54**, 17954 (1996).
  - <sup>28</sup> L. Brey and H. A. Fertig, *Phys. Rev. B* **73**, 235411 (2006).
  - <sup>29</sup> K. Wakabayashi, Y. Takane, M. Yamamoto, and M. Sigrist, *New J. Phys.* **11**, 095016 (2009).
  - <sup>30</sup> K. Wakabayashi, K. Sasaki, T. Nakanishi, and T. Enoki,

- Science and Technology of Advanced Materials **11**, 054504 (2010).
- <sup>31</sup> Studies using density function theory<sup>50,51</sup> indicate that also in the metallic armchair ribbons a narrow band-gap can be observed. However, these correlation effect go beyond the present study.
- <sup>32</sup> G. Zhang and Z. Qin, Phys. Lett. A **374**, 4140 (2010).
- <sup>33</sup> G. Zhang and Z. Qin, Chem. Phys. Lett. **516**, 225 (2011).
- <sup>34</sup> Y. Mochizuki and H. Yoshioka, J. Phys. Soc. Jpn. **78**, 123701 (2009).
- <sup>35</sup> Y. Mochizuki and H. Yoshioka, Physica E **42**, 722 (2010).
- <sup>36</sup> A. Pieper, G. Schubert, G. Wellein, and H. Fehske, Phys. Rev. B **88**, 195409 (2013).
- <sup>37</sup> Z. Li, H. Qian, J. Wu, B.-L. Gu, and W. Duan, Phys. Rev. Lett. **100**, 206802 (2008).
- <sup>38</sup> S. K. Maiti, Solid State Commun. **149**, 973 (2009).
- <sup>39</sup> H. Li and Y. Zheng, Phys. Lett. A **373**, 575 (2009).
- <sup>40</sup> M. Konôpka, J. Phys.: Condens. Matter **27**, 435005 (2015).
- <sup>41</sup> J. A. Franco-Villafañe, E. Sadurní, S. Barkhofen, U. Kuhl, F. Mortessagne, and T. H. Seligman, Phys. Rev. Lett. **111**, 170405 (2013).
- <sup>42</sup> E. Sadurní, J. A. Franco-Villafañe, U. Kuhl, F. Mortessagne, and T. H. Seligman, New J. Phys. **15**, 123014 (2013).
- <sup>43</sup> J. Munárriz Arrieta, *Modelling of Plasmonic and Graphene Nanodevices* (Springer, 2014).
- <sup>44</sup> R. Golizadeh-Mojarad and S. Datta, Phys. Rev. B **79**, 085410 (2009).
- <sup>45</sup> T. Heikkilä, *The Physics of Nanoelectronics: Transport and Fluctuation Phenomena at Low Temperatures* (Oxford University Press, 2013).
- <sup>46</sup> D. J. Klein and L. Bytautas, J. Phys. Chem. A **103**, 5196 (1999).
- <sup>47</sup> M. Bellec, U. Kuhl, G. Montambaux, and F. Mortessagne, New J. Phys. **16**, 113023 (2014).
- <sup>48</sup> Y. Shimomura, Y. Takane, and K. Wakabayashi, J. Phys. Soc. Jpn. **80**, 054710 (2011).
- <sup>49</sup> N. T. Cuong, M. Otani, and S. Okada, Phys. Rev. B **87**, 045424 (2013).
- <sup>50</sup> Y.-W. Son, M. L. Cohen, and S. G. Louie, Phys. Rev. Lett. **97**, 216803 (2006).
- <sup>51</sup> C. Motta, D. Sanchez-Portal, and M. I. Trioni, Phys. Chem. Chem. Phys. **14**, 10683 (2012).